Active harmonic filtering of islanded converter interfaced generation considering the thermal limits

Francisco Jesús Matas-Díaz
Manuel Barragán-Villarejo
José María Maza-Ortega
Department of Electrical Engineering
Universidad de Sevilla
Sevilla, Spain
{fmatas@us.es, manuelbarragan@us.es, jmmaza@us.es}

Georgios C. Kryonidis
Kyriaki-Nefeli Malamaki
Charis S. Demoulias
Department of Electrical and Computer Engineering
Aristotle University of Thessaloniki
Thessaloniki, Greece
{kryonidi@auth.gr, kyriaki_nefeli@hotmail.com, chdimoul@auth.gr}

***Abstract*—The high penetration of renewable energy sources (RES) interfaced with power electronics along with the increase of non-linear loads may create power quality problems in distribution systems. Harmonics can be mitigated by applying active filtering techniques using a virtual impedance technique and a set of resonant controllers tuned to the specific harmonics to be compensated. However, these controllers do not usually consider the thermal limits of the power converters, especially those based on the virtual impedance approach. The contribution of this paper relies on adjusting dynamically this virtual impedance to avoid the power converter overloading. The paper includes experimental results to validate the operation of the proposed algorithm.**

***Index Terms*—Power quality, converter interfaced generators, active harmonic mitigation, renewable energy sources.**

NOMENCLATURE

$\mathbf{C}$: Filter capacitor.
$\mathbf{e}_{i_{tdq}}$: ICCL (Inner Current Control Loop) current error.
$\mathbf{e}_{v_{mdq}}$: OVCL (Outer Voltage Control Loop) voltage error.
G_{ih}: ICCL resonant controller transfer function.
G_v: Virtual conductance.
G_{vh}: OVCL resonant controller transfer function.
$\mathbf{I}_r$: RMS value of the inductor current of the LC filter.
$\mathbf{I}_{rat}$: Rated current of the inverter.
$\mathbf{i}_{sdq}$: VSC injected current in dq coordinates.
$\mathbf{i}_{tdq}$: Inductor current of the LC filter in dq coordinates.
$\mathbf{i}^{\star}_{tdq}$: ICCL reference current reference in dq coordinates.
$\mathbf{i}'_{tdq}$: ICCL modified reference current in dq coordinates.
$k_{i,i}$: ICCL integral gain.
$k_{i,v}$: OVCL integral gain.
$k_{p,i}$: ICCL proportional gain.
$k_{p,v}$: OVCL proportional gain.
$k_{r,ih}$: ICCL *h-th* harmonic controller gain.
$k_{r,vh}$: OVCL *h-th* harmonic controller gain.
$\mathbf{L}_t$: Filter inductor.
$\mathbf{R}_r$: Resistance of the filter inductor.
$\mathbf{v}_{mdq}$: Capacitor voltage of the LC filter in dq coordinates.
$\mathbf{v}^{\star}_{mdq}$: OVCL voltage references.
$\mathbf{v}_{tdq}$: VSC terminal voltage in dq coordinates.
$Z^{\star}_h$: Virtual impedance for current limitation.
η_{dq}: Duty cycle of the PWM signals.
$\xi_{i_{tdq}}$: ICCL current integral error.
$\xi_{v_{mdq}}$: OVCL voltage integral error.
τ_i: ICCL time constant.
τ_v: OVCL time constant.
$\omega_{c,ih}$: ICCL *h-th* harmonic bandwidth.
$\omega_{c,vh}$: OVCL *h-th* harmonic bandwidth.
ω_h: Compensated harmonic frequency.

Funded by CERVERA Research Programme of CDTI, the Industrial and Technological Development Centre of Spain, under the research Project HySGrid+(CER-20191019) and Junta de Andalucía under the project FLEXREN (P18-TP-3655).

I. INTRODUCTION

The future of power generation will be dominated by renewable energy sources (RES). In this way, the conventional synchronous generators will be replaced with RES power plants which will be connected to the grid using converter interfaced generators (CIGs). This scenario may lead to new technical challenges affecting the secure and reliable operation of the power system [1]. This change comes along with a transition in the demand side, where traditional electromechanical loads are being replaced with power electronics. These nonlinear loads, such as variable speed motor drives, power supplies or lighting devices, introduce harmonic components. This has negative effects on the distribution system causing, among others, distorted nodal voltages [2] or transformer overheating [3].

Harmonic mitigation can be achieved by introducing passive filters [4], active power filters [5] or hybrid filters close to the most critical nonlinear loads at the cost of additional investments. Alternatively, the CIGs based on voltage source converters (VSCs) with proper control actions may help to reduce this harmonic distortion [6]. A set of resonant controllers tuned to the harmonics to be compensated, either in $\alpha\beta$ or dq coordinates, can be integrated in parallel with the main VSC current control loop for this purpose [7]. The harmonic current reference of these controllers is computed from a virtual admittance multiplied by the harmonic voltage at the point of interconnection (POI). This virtual admittance is dynamically

Citation information, DOI: 10.1109/SEST53650.2022.9898155

modified until the desired total harmonic distortion (THD) is achieved, as long as the rated current of the VSCs is not exceed. This can be considered an indirect method of harmonic voltage compensation since the variation of the virtual admittance depends on a *trial and error* methodology. In addition to this shortcoming, it is worth mentioning that the performance of this technique can be compromised in case of fast nonlinear load changes due to the time required for the computation of the virtual admittance.

On the other hand, thanks to the proliferation of microgrids and the emulation of virtual synchronous generators [8], new VSC control modes have recently emerged with the aim of controlling the POI fundamental voltage. These are commonly known as grid-former VSCs. Typically, the control strategy of a grid-former VSC is based on a cascade control with an outer voltage control loop (OVCL) and an inner current control loop (ICCL) [9]. Voltage harmonic compensation can be included in grid-former VSCs by adding a set of cascade resonant controllers for the harmonic frequencies to the fundamental frequency controller [10], [11]. In this way, any POI harmonic voltage reference can be directly tracked by the controller without the need to carry out a *trial and error* process.

The harmonic voltage references can be computed using a virtual impedance approach to improve the power sharing and the selective voltage harmonic compensation [12]. Nevertheless, it is still possible to improve the design process and the performance of the existing harmonic controllers. On the one hand, it is required to compute the resonant controller parameters to guarantee the controller stability and an adequate tracking of the harmonic references independently of the network characteristics, i.e. short-circuit power and R/X ratio [13]. On the other hand, in cascade controllers the OVCL generates current references to ICCL. This means that the current reference value is unknown in advance, which could lead to the VSC overload. For the fundamental frequency OVLC, a saturation is usually added to the current reference in order to limit its value below the VSC rated current. However, no strategy can be found in the literature for cascade controllers dealing with harmonic components.

The main contribution of this paper is the definition of a harmonic voltage controller for grid-forming VSCs which prevents its overloading. To this end, a set of resonant cascade controllers for harmonic voltage compensation are added to the fundamental frequency POI voltage control [14]. The controller harmonic reference voltage is set by means of an adaptive virtual impedance that is modified considering the POI injected current to avoid the VSC overload. Therefore, this paper can be considered an extension of the previous work [14] for harmonic compensation in grid-forming VSC.

The rest of the paper is organized as follows. Section II presents the proposed control strategy to bring harmonic mitigation within the VSC thermal limits. Section III outlines a sensitivity analysis to analyze the influence of the controller parameters. Section IV provides the experimental validation of the proposal. Finally, the paper closes with the main conclusions.

II. Active Harmonic Filtering Controller

This section outlines the proposed control algorithm shown in Fig. 1. This controller is composed of three main blocks which are analyzed in the following subsections.

A. Fundamental voltage control

The objective of this controller is to set the fundamental POI voltage, $\mathbf{v}_{mdq,1}$, to a given reference. To achieve this goal, a proportional-integral (PI) cascade controller in dq coordinates composed of an OVCL and an ICCL is proposed. The gains of both control loops are usually tuned to avoid dynamic interactions between them. This objective is achieved by setting the OVCL time constant at least ten times slower than the ICCL one. In order to guarantee that each control loop respects a desired time constant, a negative feedback through a virtual conductance G_v is added for modifying the ICCL current reference [14]. In this way, both control loops respond as a first-order system with the specified time constant. The most important variables and parameters of the proposed cascade control are summarized in the Nomenclature section. The OVCL computes the modified inductor current reference, $\mathbf{i}'_{tdq}$, as follows:

$$\mathbf{i}^{\star}_{tdq} = k_{p,v} \cdot \mathbf{e}_{v_{mdq}} + k_{i,v} \cdot \xi_{v_{mdq}} + \mathbf{C}_{dq}\omega \cdot \mathbf{v}_{mqd} + \mathbf{i}_{s,dq} \quad (1)$$

$$\mathbf{i}'_{tdq} = \mathbf{i}^{\star}_{tdq} - G_v \mathbf{v}_{mdq} \quad (2)$$

where $\mathbf{C}_{dq} = diag\,[-C\ C]$. Then, this current reference is used by the ICCL to compute the required VSC terminal voltage, $\mathbf{v}_{tdq}$, as:

$$\mathbf{v}_{tdq} = k_{p,i} \cdot \mathbf{e}_{i_{tdq}} + k_{i,i} \cdot \xi_{i_{tdq}} + \mathbf{L}_{tdq}\omega \cdot \mathbf{i}_{tqd} + \mathbf{v}_{mdq} \quad (3)$$

where $\mathbf{L}_{t,dq} = diag\,[-L_t\ L_t]$. The gains of these PI controllers can be computed as a function of the controller time constants τ_i and τ_v as:

$$k_{p,i} = \frac{L_t}{\tau_i} \quad k_{i,i} = \frac{R_t}{\tau_i} \quad k_{p,v} = \frac{C}{\tau_v} \quad k_{i,v} = \frac{G_v}{\tau_v}. \quad (4)$$

B. Harmonic voltage control

A set of cascade resonant controllers per each compensated harmonic are added in parallel to the fundamental voltage control. These resonant controllers entail a modification of the inductor reference current, $\mathbf{i}'_{tdq}$, and the VSC terminal voltage, $\mathbf{v}_{tdq}$, given by (1) and (3) respectively as shown in Fig. 1. The transfer functions G_{vh} and G_{ih} of each of these resonant controllers are formulated as:

$$G_{vh} = \sum_h \frac{k_{r,vh}s}{s^2 + \omega_{c,vh}s + \omega_h^2}\ ;\ G_{ih} = \sum_h \frac{k_{r,ih}s}{s^2 + \omega_{c,ih}s + \omega_h^2} \quad (5)$$

where ω_h is the compensated harmonic frequency considering the synchronous rotation of the dq reference frame where the controller is formulated.

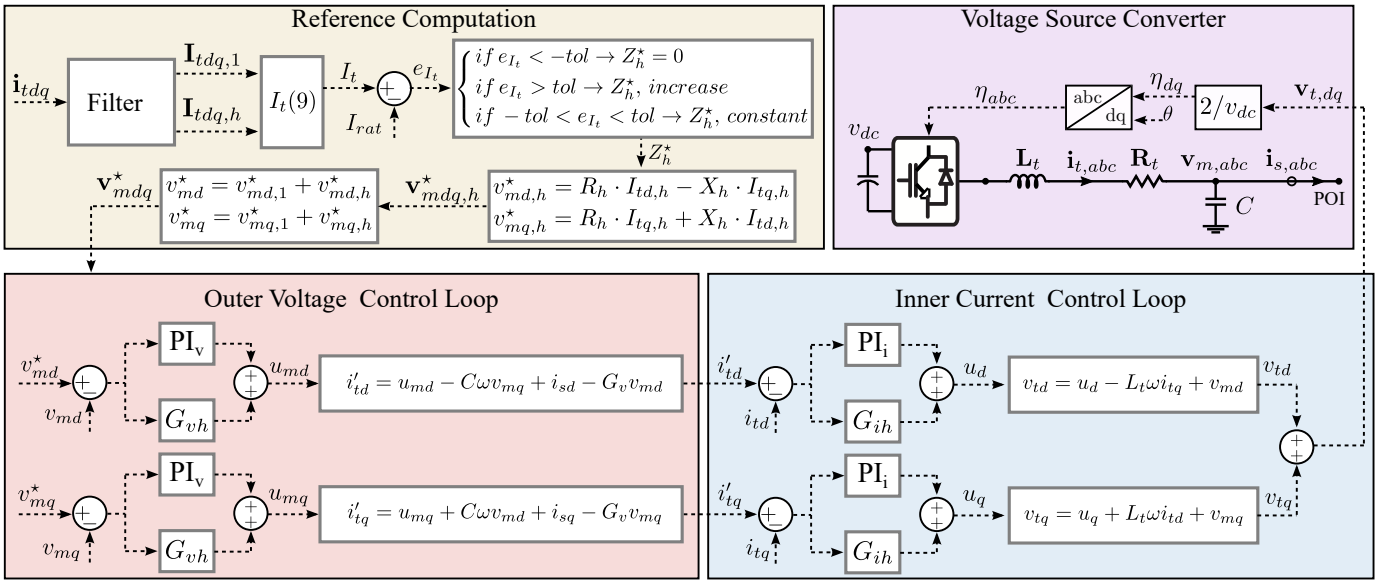

Fig. 1. Proposed cascade control for fundamental and harmonic frequencies in dq coordinates for grid–forming LC–coupled VSCs.

C. Virtual impedance for VSC overloading protection

The resonant controllers guarantee a null *h-th* harmonic POI voltage if the corresponding reference $\mathbf{v}^\star_{mdq,h}$ is set to zero. However, this performance is achieved thanks to a VSC *h-th* harmonic current injection which may cause a VSC overload if the VSC current limit is not considered. To avoid the VSC damage, it is proposed to add a virtual impedance $Z_h^\star$ in charge of setting a harmonic voltage reference $\mathbf{v}^\star_{mdq,h}$ for limiting the VSC harmonic current if required. This harmonic voltage reference is computed as:

$$v^\star_{md,h} = I_{td,h} \cdot R_h - I_{tq,h} \cdot X_h \tag{6}$$

$$v^\star_{mq,h} = I_{tq,h} \cdot R_h + I_{td,h} \cdot X_h \tag{7}$$

where R_h and X_h are the virtual resistance and reactance. Note that $\mathbf{I}_{tdq,h}$ can be calculated using a moving average filter [15].

The virtual impedance depends on the RMS value of the VSC injected current which is computed as:

$$I_t = \frac{1}{\sqrt{2}}\sqrt{I^2_{td,1} + I^2_{tq,1} + \sum_h I^2_{td,h} + \sum_h I^2_{tq,h}} \tag{8}$$

where $I_{td,1}$, $I_{tq,1}$, $I_{td,h}$ and $I_{tq,h}$ are the amplitudes of the fundamental and harmonic currents in dq coordinates. Note that the virtual impedance is set to zero if I_t is lower than the VSC rated current, I_{rat}. Consequently, the harmonic voltage reference is zero since the VSC has enough capacity to inject the required harmonic current to completely mitigate the POI harmonic voltages. Nevertheless, if I_t is greater than I_{rat}, the VSC overload is produced and the harmonic voltage reference must be set to a non-null value to reduce the harmonic current injection. In such a case, it is proposed to linearly increase the harmonic virtual impedance to achieve a VSC injected current lower than I_{rat}. Taking into account that the harmonic virtual impedance is defined as a piece-wise linear function, it is incorporated a hysteresis band with a given tolerance to limit the impedance variations as shown in Fig. 1. With this regard, e_{I_t} computes the difference between I_t and I_{rat} to decide the virtual impedance value. Finally, the R/X ratio of the virtual impedance is adjusted as a function the network where the VSC is connected to.

III. Sensitivity analysis

The aim of this section is to evaluate the stability and dynamic performance of the proposed controller in the frequency domain. In order to simplify the analysis, the cross–coupling cancellation terms have been omitted in this analysis. This simplification leads to the same dynamic system for d and q coordinates. The computation of the transfer functions has been done using the parameters collected in Table I which are expressed in per unit to obtain general conclusions irrespective of the converter rated magnitudes. Note that the analysis has been particularized for compensating the 6^{th} harmonic in the dq reference frame which corresponds to the negative and positive sequences of the 5^{th} and 7^{th} harmonics in the abc reference frame respectively.

The closed-loop transfer function (CLTF) of the system $G_{CLTF} = v_m/v_m^\star$ can be modeled as:

$$G_{CLTF} = \frac{1}{\frac{1+(PI_i+G_{ih})G_{LC}}{(PI_v+G_{vh})(PI_i+G_{ih})G_{LC}} + 1} \tag{9}$$

where,

$$PI_v = k_{p,v} + \frac{k_{i,v}}{s}\ ;\ PI_i = k_{p,i} + \frac{k_{i,i}}{s} \tag{10}$$

$$G_{LC} = \frac{1}{L_tCs^2 + (G_vL_t + R_tC)s + R_tG_v + 1} \tag{11}$$

The amplitude of this closed-loop transfer function is shown in the top plot of Fig. 2 where it can be noticed the high gain

TABLE I
PARAMETERS OF THE SENSITIVITY ANALYSIS

Parameter	Value	Parameter	Value
L_t	0.1 p.u.	R_t	0.01 p.u.
C	0.01 p.u.	G_v	0.01 p.u
τ_i	0.25 ms	τ_v	2.5 ms
$k_{r,ih}$	120	$\omega_{c,ih}$	0.02ω
$k_{r,vh}$	120	$\omega_{c,vh}$	0.002ω

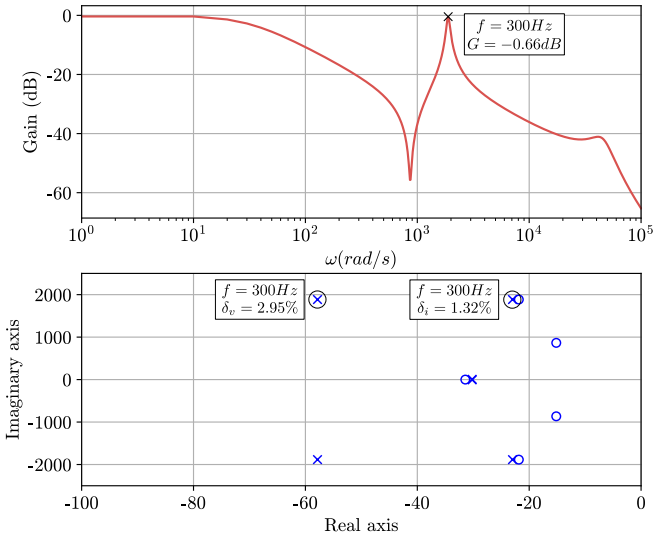

Fig. 2. Frequency-domain analysis of the closed-loop system response G_{CLTF}. Top plot: Bode diagram. Bottom plot: Root locus.

at the 6^{th} harmonic. The bandwidth of the resonant terms has been limited enough in order to reduce the amplification of adjacent harmonics. These non-zero bandwidth terms, $\omega_{c,ih}$, $\omega_{c,vh}$ in (5), cause a slight gain drop at the resonant frequency but, in turn, provide damping to the system. This is observed in the root locus of the closed-loop transfer function shown in the bottom plot of Fig. 2 where the damping at the 6^{th} harmonic of the OVCL and ICCL, δ_v and δ_i, are detailed.

IV. EXPERIMENTAL VALIDATION

A. Description of the testbed and controller parameters

The experimental setup used to validate the proposed control algorithm is shown in Fig. 3. This testbed consists of a three–phase three–wire VSC with a DC voltage source connected to its DC side. The AC side is connected to the POI through a LC filter where a set of switched resistive and nonlinear loads are connected. The relevant parameters of the hardware components and the proposed controller are summarized in Table II. The control algorithm is embedded in a Delfino TMS320F28335 DSP from Texas Instruments, with a sampling frequency of 20 kHz and a switching frequency of 10 kHz.

For the experimental results, a single 6^{th} harmonic resonant controller in dq coordinates is added to the fundamental frequency which compensates the negative sequence of the

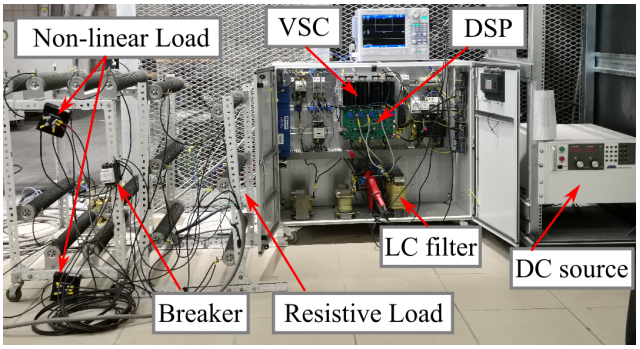

Fig. 3. Laboratory experimental test bench.

TABLE II
PARAMETERS OF THE EXPERIMENTAL SETUP AND CONTROLLER GAINS

Parameter	Value	Parameter	Value
v_{dc}	730 V	v_{rat}	400 V
I_{rat}	20 A	L_t	2.5 mH
C	4 μF	R_1	50 Ω
R_{dc}	100 Ω	G_v	0.08 S
τ_v	2.5 ms	τ_i	0.25 ms
$k_{p,v}$	0.0016	$k_{p,i}$	10
$k_{i,i}$	314.1592	$k_{i,v}$	32
$k_{r,v6}$	120	$k_{r,i6}$	120
$\omega_{c,vh}$	37.70	$\omega_{c,ih}$	3.77

harmonic 5^{th} and the positive sequence of the harmonic 7^{th} in abc coordinates.

B. Experimental results

The experimental tests carried out to validate the proposed performance focus both in steady-state and transient conditions.

Regarding the steady-state performance, *Test 1* and *Test 2* show the controller performance without and with the harmonic voltage control respectively. The harmonic voltage reference has been set to zero. Fig. 4 shows the POI voltage, $\mathbf{v}_{mabc}$, and the injected VSC currents, $\mathbf{i}_{sabc}$, for *Test 1*. It can be clearly noticed the high voltage harmonic distortion due to the harmonics of the nonlinear load as shown also in Table III. The activation of the harmonic frequency mitigation in *Test 2* leads to a drastic reduction of the 5^{th} and 7^{th} harmonic voltages as depicted in Table III. The POI voltage, however, is still distorted as shown in Fig. 5 because just one controller tuned to the 5^{th} and 7^{th} harmonics has been incorporated.

Two additional tests have been carried out to evidence the performance of the proposed controller in transient state. Particularly, *Test 3* analyzes the transient response where the nonlinear load is added to the resistive load being the harmonic voltage controller activated with the harmonic virtual impedance set to zero. Before the connection of the nonlinear load, currents and voltages are almost sinusoidal with a very low THD as shown in Table III, evidencing the good performance of the fundamental voltage controller. When the nonlinear load is connected, a fast response of the harmonic

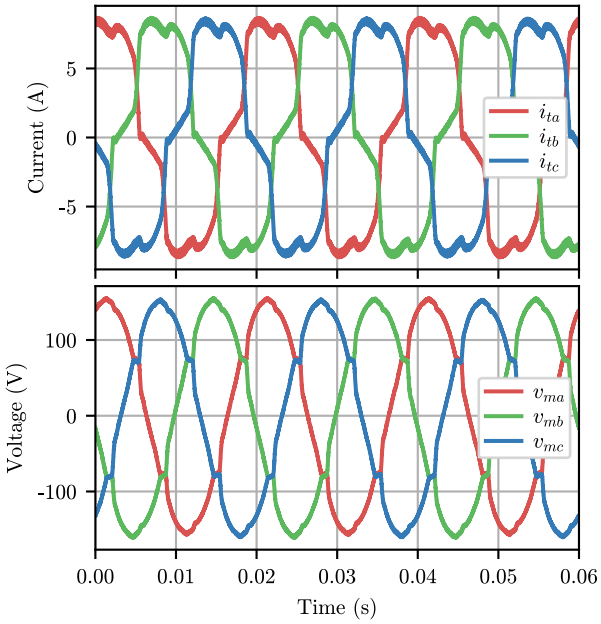

Fig. 4. *Test 1*. Steady-state three-phase currents and voltages without harmonic compensation.

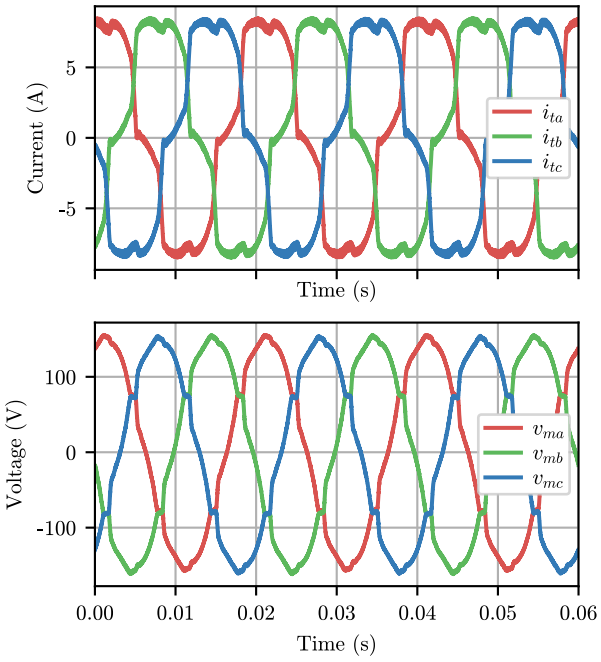

Fig. 5. *Test 2*. Steady-state three-phase currents and voltages with harmonic compensation.

voltage controller is observed. The action of the resonant control mitigates the 5^{th} and 7^{th} harmonic voltages as shown in Table III. However, the voltage THD increases with respect to the initial situation since no compensation for other major harmonics (11^{th}, 13^{th}, etc.) demanded by the non-linear load has been included.

Finally, *Test 4* implements the proposed controller following

TABLE III
THD, 5^{th} AND 7^{th} HARMONICS IN THE EXPERIMENTAL TESTS.

Test	THD_I	I_5	I_7	THD_V	V_5	V_7
Test 1	17.81	15.43	5.98	5.75	3.27	1.95
Test 2	17.41	14.72	6.33	4.47	0.18	0.12
Test 3 ($t = 0.16$ s.)	0.70	0.08	0.04	0.51	0.04	0.04
Test 3 ($t = 0.22$ s.)	17.41	14.69	6.31	4.74	0.12	0.08
Test 4 $R_h = 0\,\Omega$	22.95	20.69	7.22	6.83	2.43	1.09
Test 4 $R_h = 6.47\,\Omega$	17.98	15.47	7.69	9.34	7.79	3.32

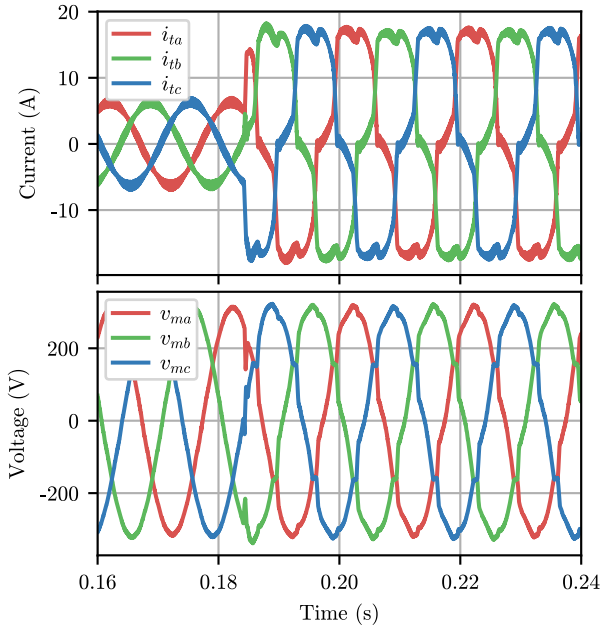

Fig. 6. *Test 3*. Transient response of the three-phase currents and voltages with harmonic compensation.

a Hardware-in-the-Loop (HIL) approach. This HIL test has been conducted instead of the experimental testbed due to the impossibility of reaching the VSC thermal limit with the already available loads in the laboratory. Particularly, the Typhoon HIL 402-01-005 platform has been used to evaluate the performance in case of a non-null value of the virtual impedance. As the VSC is connected to a predominantly resistive network, the virtual impedance will contain only the resistive term. The tolerance term of the hysteresis band has been set to 0.4 A.

The RMS VSC current and the virtual resistance for this *Test 4* are depicted in Fig. 7. At $t = 1.2$ s, the nonlinear load is drastically increased leading to a RMS current higher than the VSC rated current. Therefore, the value of the virtual resistance starts to increase in order to reduce the injected harmonic current. Note that the VSC current is decreased linearly as the virtual resistance is increased. The value of the virtual resistance stabilizes in 6.47 Ω when the current is introduced within the controller tolerance margin. Consequently, this non-zero virtual resistance leads to a non-null harmonic voltage reference which increases the 5^{th} and 7^{th} harmonic voltages

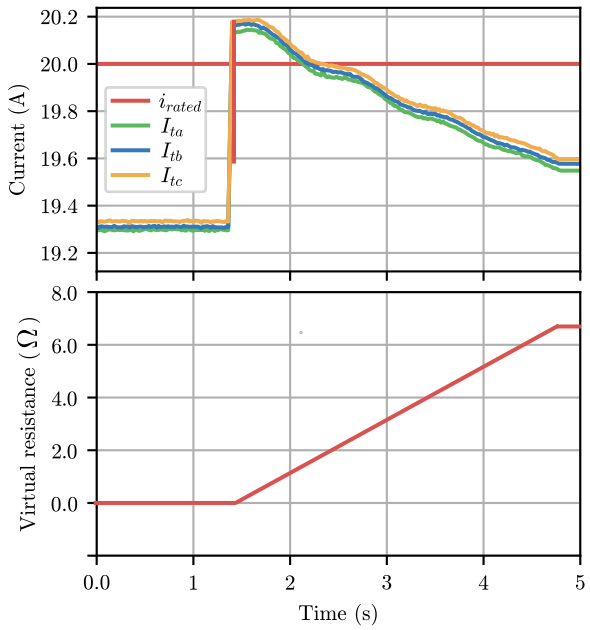

Fig. 7. RMS current and virtual resistance for *Test 4* under overload situation.

as shown in Table III.

V. Conclusion

This paper has presented a virtual impedance strategy to limit the active harmonic filtering capability of islanded grid-forming CIGs in case of converter overload. The objective is to establish a harmonic voltage reference as a function of the injected VSC current and a virtual impedance in order to limit the VSC current below its rated current. To achieve this objective, a set of resonant controllers tuned to the selected harmonic frequencies are added in parallel to the OVCL and ICCL of the fundamental frequency controller. A sensitivity analysis has been introduced in the frequency domain to evaluate the dynamic performance and stability of the proposed controller.

The proposal has been experimentally validated in a laboratory testbed through several test cases in steady-state and transient conditions. The performance of the controller has been evaluated through the analysis of the selected harmonic frequencies and THD of the VSC voltages and currents. The steady-state results show that the controller is able to completely eliminate the harmonic components tuned within the resonant controllers. In addition, the proposed controller shows a good dynamic response in transient conditions due to sudden load changes. Finally, with respect to VSC overload situations, the virtual impedance strategy has demonstrated its ability to maintain the VSC currents within the permissible technical limits in the event that harmonic voltage compensation leads to an excessive harmonic current injection.

Future research lines will extend this strategy to grid-feeding and grid-forming VSCs operating in grid-connected mode. For this purpose, it will be key to reformulate the sensitivity analysis to consider the network parameters in order to analyze how the different controller settings influence the dynamic performance and stability. In addition, the experimental tests involving the HIL approach will be implemented in the laboratory by incorporating new loads to reach the VSC thermal limit.

References

[1] D. Liu, X. Zhang, and C. K. Tse, "Effects of high level of penetration of renewable energy sources on cascading failure of modern power systems," *IEEE Journal on Emerging and Selected Topics in Circuits and Systems*, vol. 12, no. 1, pp. 98–106, 2022.

[2] A. Huda and R. Živanović, "Large-scale integration of distributed generation into distribution networks: Study objectives, review of models and computational tools," *Renewable and Sustainable Energy Reviews*, vol. 76, pp. 974–988, 09 2017.

[3] D. Kumar and F. Zare, "Harmonic Analysis of Grid Connected Power Electronic Systems in Low Voltage Distribution Networks," *IEEE Journal of Emerging and Selected Topics in Power Electronics*, vol. 4, pp. 70–79, 03 2016.

[4] J. C. Churio-Barboza and J. M. Maza-Ortega, "Comprehensive design methodology of tuned passive filters based on a probabilistic approach," *IET Generation, Transmission & Distribution*, vol. 8, no. 1, pp. 170–177, 2014.

[5] M. El-Habrouk, "Active power filters: A review," *IEE Proceedings - Electric Power Applications*, vol. 147, pp. 403–413(10), September 2000.

[6] X. Liang and C. Andalib Bin-Karim, "Harmonics and mitigation techniques through advanced control in grid-connected renewable energy sources: A review," *IEEE Transactions on Industry Applications*, vol. 54, no. 4, pp. 3100–3111, 2018.

[7] N. Pogaku and T. Green, "Harmonic mitigation throughout a distribution system: a distributed-generator-based solution," *IEE Proceedings-Generation, Transmission and ...*, vol. 151, no. 3, pp. 201–212, 2004.

[8] G. C. Kryonidis, K.-N. D. Malamaki, J. M. Mauricio, and C. S. Demoulias, "A new perspective on the synchronverter model," *International Journal of Electrical Power & Energy Systems*, vol. 140, p. 108072, 2022.

[9] Q. Lei, F. Z. Peng, and S. Yang, "Multiloop control method for high-performance microgrid inverter through load voltage and current decoupling with only output voltage feedback," *IEEE Transactions on Power Electronics*, vol. 26, no. 3, pp. 953–960, 2011.

[10] A. Micallef, M. Apap, C. Spiteri-Staines, and J. M. Guerrero, "Mitigation of Harmonics in Grid-Connected and Islanded Microgrids Via Virtual Admittances and Impedances," *IEEE Transactions on Smart Grid*, vol. 8, no. 2, pp. 651–661, 2017.

[11] M. Barragán-Villarejo, J. M. Mauricio, J. C. Olives-Camps, F. J. Matas-Díaz, F. de Paula García-López, and J. M. Maza-Ortega, "Harmonic and imbalance compensation in grid-forming vsc," in *2020 IEEE International Conference on Industrial Technology (ICIT)*, pp. 757–762, 2020.

[12] A. Micallef, M. Apap, C. Spiteri Staines, and J. Guerrero, "Selective virtual capacitive impedance loop for harmonic voltage compensation in islanded microgrids," 11 2013.

[13] X. Wang and F. Blaabjerg, "Harmonic Stability in Power Electronic-Based Power Systems: Concept, Modeling, and Analysis," *IEEE Transactions on Smart Grid*, vol. 10, no. 3, pp. 2858–2870, 2019.

[14] F. J. Matas-Diaz, M. Barragán-Villarejo, J. C. Olives-Camps, J. M. Maurcio, and J. M. Maza-Ortega, "Virtual conductance based cascade voltage controller for VSCs in islanded operation mode," *Journal of Moder Power Systems and Clean Energy*, vol. Accepted for publication, 2022.

[15] J. M. Maza-Ortega, J. A. Rosendo-Macias, A. Gómez-Expósito, S. Ceballos-Mannozzi, and M. Barrágan-Villarejo, "Reference current computation for active power filters by running dft techniques," 2010.